Clinical Pharmacokinetics (2020) 59:207–216
https://doi.org/10.1007/s40262-019-00803-y

ORIGINAL RESEARCH ARTICLE

A Semi-Mechanistic Population Pharmacokinetic/Pharmacodynamic Model of Bortezomib in Pediatric Patients with Relapsed/Refractory Acute Lymphoblastic Leukemia

Julie M. Janssen[1] · T. P. C. Dorlo[1] · D. Niewerth[2] · A. J. Wilhelm[3] · C. M. Zwaan[4,5,16] · J. H. Beijnen[1,6] · A. Attarbaschi[7,8] · A. Baruchel[9,16] · F. Fagioli[10] · T. Klingebiel[11] · B. De Moerloose[12] · G. Palumbo[13] · A. von Stackelberg[14] · G. J. L. Kaspers[2,4] · A. D. R. Huitema[1,15]

Published online: 16 July 2019

Abstract

Introduction The pharmacokinetics (PK) of the 20S proteasome inhibitor bortezomib are characterized by a large volume of distribution and a rapid decline in plasma concentrations within the first hour after administration. An increase in exposure was observed in the second week of treatment, which has previously been explained by extensive binding of bortezomib to proteasome in erythrocytes and peripheral tissues. We characterized the nonlinear population PK and pharmacodynamics (PD) of bortezomib in children with acute lymphoblastic leukemia.

Methods Overall, 323 samples from 28 patients were available from a pediatric clinical study investigating bortezomib at an intravenous dose of 1.3 mg/m^2 twice weekly (Dutch Trial Registry number 1881/ITCC021). A semi-physiological PK model for bortezomib was first developed; the PK were linked to the decrease in 20S proteasome activity in the final PK/PD model.

Results The plasma PK data were adequately described using a two-compartment model with linear elimination. Increased concentrations were observed in week 2 compared with week 1, which was described using a Langmuir binding model. The decrease in 20S proteasome activity was best described by a direct effect model with a sigmoidal maximal inhibitory effect, representing the relationship between plasma concentrations and effect. The maximal inhibitory effect was 0.696 pmol AMC/s/mg protein (95% confidence interval 0.664–0.728) after administration.

Conclusion The semi-physiological model adequately described the nonlinear PK and PD of bortezomib in plasma. This model can be used to further optimize dosing of bortezomib.

Key Points

An increase in pediatric exposure to bortezomib was observed in the second week of treatment, presumably caused by saturable binding in erythrocytes.

This analysis provides the first population-based analysis combining the pharmacodynamics and time-dependent pharmacokinetics of bortezomib.

✉ Julie M. Janssen
ju.janssen@nki.nl

Extended author information available on the last page of the article

1 Introduction

The 5-year overall survival of children with acute lymphoblastic leukemia (ALL) exceeds 85% after primary treatment. However, relapse occurs in approximately 15–20% of patients, and only 40% of relapsing patients can be cured, mainly as a result of emerging resistance to conventional chemotherapy [1]. To improve the treatment options for pediatric malignancies, the development of new anticancer drugs is essential. Novel anticancer agents inhibiting specific molecular targets have promise to overcome resistance to previously administered therapy, and to enhance survival rates [2].

Bortezomib is a small dipeptidyl boronic acid exhibiting reversible inhibitory effects on the chymotrypsin-like proteolytic activity of the 20S proteasome. By binding the 20S proteasome, bortezomib interferes with the

ubiquitin–proteasome pathway, which plays a pivotal role in the degradation of proteins involved in tumor cell proliferation and cell survival [3, 4]. Bortezomib is registered for the treatment of adults with multiple myeloma (MM) as a 2-weekly schedule of 1.3 mg/m^2 intravenously on days 1, 4, 8, and 11 [3]. The results from preclinical and in vivo studies showed high antileukemic activity of bortezomib towards ALL cell lines [5].

Bortezomib pharmacokinetics (PK) have been studied in adults with relapsed MM and are characterized by a large volume of distribution and rapid decline in plasma concentrations within the first hour after administration. In addition, a marked increase in bortezomib exposure associated with a decrease in clearance was observed in the second week of treatment [4, 6]. The pharmacodynamic (PD) effect of bortezomib can be measured by 20S proteasome activity in whole blood. In adults, a rapid inhibition of 20S proteasome activity directly after drug administration was observed. Inhibition levels followed systemic exposure and declined with decreasing plasma concentrations. In accordance with the PK observations, the maximum 20S proteasome inhibition was higher in the second week of treatment [4, 6]. In several pediatric studies with a limited number of patients, bortezomib PK and PD were shown to be similar to that observed in adults [7–9]. A recently developed population PK model confirmed these results in a larger group of pediatric patients [10]; however, a semi-mechanistic characterization of the nonlinear PK behavior in children has not yet been published.

We previously conducted a phase II clinical trial investigating bortezomib in pediatric patients with ALL, where bortezomib was administered in a twice-weekly 1.3 mg/m^2 dosing schedule. Clinical results of this study have been presented earlier [11]. The primary goal of the population PK analysis that we present here was to characterize the time-dependent PK/PD profile of bortezomib in pediatric patients in a semi-physiological approach to better understand the processes driving observed nonlinearities.

2 Methods

2.1 Patients, Sampling and Analytical Methodology

An open-label, randomized, feasibility, phase II study combining bortezomib with conventional chemotherapy for the treatment of pediatric patients with relapsed/refractory ALL (rALL) was conducted by the Innovative Therapies for Children with Cancer (ITCC) consortium (Dutch National Trial Registry number 1881/ITCC021) [11]. The primary aim of this clinical study was to assess the antileukemic activity of bortezomib in combination with conventional chemotherapy in pediatric rALL. All patients were repeatedly treated with bortezomib at an intravenous dose of 1.3 mg/m^2 in a 2-week cycle, and were randomized to receive bortezomib on days 1, 4, 8, and 11 in arm A, or on days 8, 11, 15, and 18 in arm B. Patients were additionally treated with standard re-induction chemotherapy consisting of 2 weeks of dexamethasone combined with two injections of vincristine administered once weekly, and with intrathecal administration of methotrexate. Samples for PK and PD assessment were collected after the first and third administration days of the first cycle after the start of treatment at time points predose and 15 min, 3, 8, 24, 48, and 72 h after dose. An additional sample was taken 30 min after dose on the second administration day. Demographic characteristics such as age, sex, total body weight, and height were recorded at the start of treatment. Informed consent was obtained from all individual participants or their legal guardians.

After collection, peripheral blood samples for PK analysis were centrifuged at 4 °C for 10 min at 1000 g, and plasma was stored at −70 °C until analysis. Separation between metabolites and interfering endogenous compounds and detection was achieved by liquid chromatography–tandem mass spectroscopy (LC–MS/MS) using a Waters Xbridge Shield RP18/50 × 2.1 mm, 3.5 µm column at 40 °C, and using a ternary gradient of 0.1% formic acid in water as mobile phase A, acetonitrile as mobile phase B, and 2-pro panol:acetonitrile:water:ammonia (30:30:40:2, v/v/v/v) as mobile phase C. The initial flow rate was 0.40 mL/min. A Sciex 4000 quadrupole mass spectrometer equipped with a turbo ion spray source was used for detection in the positive ion model. Quantification was based on multiple reaction monitoring of the transitions of *m*/*z* 367.2–226.2 for bortezomib and 376.3–234.2 for its internal standard. A linear calibration curve with a $1/x^2$ weighting factor ranging from 0.1 to 25.0 ng/mL was used.

The 20S proteasome activity was determined by measuring the rate of proteolytic hydrolysis of a fluorescent tagged peptide substrate Suc-Leu-Leu-Val-Tyr-AMC, in a lysate prepared from peripheral whole blood samples. The activity was normalized to the amount of protein present in the sample lysate. Protein concentrations were determined using a Pierce BCA Protein Assay Kit ($R^2 > 0.99$), and the specific activity of each sample was determined against an AMC standard curve.

2.2 Model Development

2.2.1 Structural Model

For a description of the PK of bortezomib, one- to three-compartment models were evaluated using the bortezomib concentrations that were measured in plasma (C_{plasma}). Previously, binding of bortezomib to erythrocytes was suggested [12]. A semi-physiological approach was tested

to describe this distribution, using the Langmuir equation for saturable binding equilibriums (Eq. 1).

$$C_{\text{bound}} = \frac{B_{\max} \cdot C_{\text{plasma}}}{C_{\text{plasma}} + K_{\text{D}}}, \quad (1)$$

where $B_{\max}$ (ng/mL) corresponds to the maximal binding capacity, and K_{D} (ng/mL) is the equilibrium dissociation constant, i.e. if the plasma concentration is equal to K_{D}, the bound concentration (C_{bound}) is half maximal. It was assumed that the distribution of bortezomib within the central compartment occurred instantaneously. Hence, the fractions of erythrocyte bound and unbound bortezomib in whole blood and plasma, respectively, were assumed to be in equilibrium at any moment.

Total body weight (WT) was included in the PK model a priori using allometric scaling. All clearance and volume parameters were scaled to the median body weight in the dataset (i.e. 32 kg). The allometric exponents were fixed to 0.75 for clearance parameters, and 1 for volumes of distribution, according to allometric principles (Eqs. 2 and 3) [13].

$$P_{\text{CL}} = P0_{\text{CL}} \cdot \left(\frac{WT}{32}\right)^{0.75}, \quad (2)$$

$$P_{\text{V}} = P0_{\text{V}} \cdot \left(\frac{WT}{32}\right), \quad (3)$$

where P represents the body weight-adjusted population parameter, and $P0$ represents the baseline population parameter estimate for parameter P. For all patients, body weight at baseline was available.

An additional effect of maturation on clearance was also explored by extending Eqs. 1–4 [14, 15].

$$P_{\text{CL}} = P0_{\text{CL}} \cdot \left(\frac{WT}{32}\right)^{0.75} \cdot \frac{\text{PMA}^{\text{Hill}}}{\text{PMA}_{50}^{\text{Hill}} + \text{PMA}^{\text{Hill}}}, \quad (4)$$

where PMA_{50} is the postmenstrual age (PMA; gestational plus postnatal age) at which clearance reached 50% maturity, and Hill is the shape parameter.

Sequential modeling of the PK and PD was used to determine the PK/PD model. The PD model was developed using the typical parameters from the final PK model as input, simulating individual bortezomib concentrations [16]. Models using either simulated C_{plasma} or C_{bound} as PK drivers were explored. Exploratory plots were used to determine the relationship between the PK and the decreases in 20S proteasome activity after bortezomib administration. Linear, maximal inhibitory effect ($E_{\max}$) and sigmoidal $E_{\max}$ relationships between PK and 20S proteasome activity were investigated. Weight, sex and treatment arms were assessed as covariates for clinical and statistical significance.

2.2.2 Stochastic Model

Between-subject variability (BSV) and within-subject variability (WSV) were evaluated for all parameters using an exponential error model (Eq. 5):

$$P_i = P_{\text{pop}} \cdot \exp\left(\eta_{i,\text{BSV}} + \eta_{i,\text{WSV}}\right), \quad (5)$$

where P_i represents the individual parameter estimate for individual i, P_{pop} represents the typical population parameter estimate, η_i represents either the BSV or WSV effect for individual i, and where η_i was assumed to be normally distributed following $N\,(0,\, \sigma^2)$. Occasions were defined as individual treatment weeks, in which week 1 consists of the first and second bortezomib administration, and week 2 consists of the third and fourth administration.

Residual unexplained variability was described using a proportional error model (Eq. 6):

$$C_{\text{obs},ij} = C_{\text{pred},ij} \cdot (1 + \varepsilon_{p,ij}), \quad (6)$$

where $C_{\text{obs},ij}$ represents the observed concentration for individual i and observation j, $C_{\text{pred},ij}$ represents the individual predicted concentration, and $\varepsilon_{p,ij}$ represents the proportional error distributed following $N\,(0,\, \sigma^2)$.

2.3 Model Selection and Evaluation

The model selection criteria were the same for both the PK and PD analyses. Discrimination between models was guided by physiological plausibility, goodness-of-fit (GOF) plots, precision of parameter estimates, and change in objective function value (OFV). A drop of ≥ 6.63, corresponding to $p < 0.01$ (Chi-square distribution with 1 degree of freedom), was considered a significant improvement in the fit for hierarchical models. The adequacy of the models was assessed using GOF plots and prediction-corrected visual predictive checks (pcVPC) [17]. Parameter precision was obtained by sampling importance resampling (SIR) [18].

2.4 Software

Nonlinear mixed-effects modeling was performed using NONMEM® version 7.3 (ICON Development Solutions, Ellicott City, MD, USA) and Perl-speaks-NONMEM (PsN, version 4.4.8), with first-order conditional estimation with interaction (FOCE-I) as the estimation method. Piraña version 2.9.7 was used as the graphical user interface for NONMEM [19–21], and R version 3.4.3 was used for processing the data, graphical diagnostics, and simulation purposes [22].

3 Results

3.1 Patients and Data

A total of 323 PK plasma samples and 356 PD whole blood samples from 28 patients were included in the final analysis data set. The median number of bortezomib plasma concentrations available per patient was 13 (range 4.0–14.0) and the median number of 20S proteasome activity samples was 15 (range 5.0–16.0). The patient characteristics are depicted in Table 1. The overall mean age at baseline was 9.94 years (range 1.0–17.6) and the mean weight at baseline was 34.4 kg (range 7.8–69.7). The clinical results have been described in detail by Kaspers et al. [11]

3.2 Population Pharmacokinetic Analysis

A quick decrease in bortezomib plasma concentrations was observed within 1 h after administration. The observed concentration-time profiles were well-described using a two-compartment model with first-order elimination. Total body weight was included a priori as an allometric function for body size effect on all parameters; an additional maturation effect could not be identified. In addition, sex could not be identified as a covariate that affected the PK in our population.

To explore the marked difference in plasma concentrations between the first and second treatment weeks, an empirical approach was used first. Clearance and volume of distribution parameters were estimated separately for both treatment weeks, showing that the central and peripheral volumes of distribution were notably larger in the first week of treatment. No difference in clearance was found between the 2 weeks. Saturable nonspecific binding of bortezomib in the central compartment was introduced in the model and resulted in a strong improvement in model fit (difference in OFV = – 80). Furthermore, with the introduction of saturable binding, the decrease in volume of distribution during treatment disappeared. The parameter estimates for the final model are summarized in Table 2. The clearance of bortezomib from the central compartment was estimated at 6.32 L/h (95% confidence interval (CI) 3.76–9.83). Volumes of distribution were large, i.e. 68.8 L (95% CI 44.7–104) and 622 L (95% CI 388–1102) for the central and peripheral volumes of distribution, respectively. Figure 1 shows a schematic representation of the semi-physiological model. The relationship between C_{bound} and C_{plasma} within the central compartment was well-described using the Langmuir equation. B_{max} was estimated at 60.4 ng/mL (95% CI 34.4–105) and K_D was estimated at 60.6 ng/mL (95% CI 33.4–113). The model included BSV on B_{max}, which was estimated as 51.8% (95% CI 39.2–70.7). The introduction of BSV on the remaining structural parameters resulted in overparameterization of the model. In addition, the incorporation of WSV did not result in a significant improvement of the model. Residual unexplained variability was characterized by a proportional error [percentage coefficient of variation (CV%)] of 68.1% (95% CI 63.1–74.1).

3.3 Population Pharmacodynamic Analysis

A quick decrease in 20S proteasome activity directly after administration of bortezomib, with recovery to baseline before administration of the following dose, was observed. This decrease was adequately described using a direct effect inhibitory sigmoidal E_{max} model with proportional error. The relationship between drug exposure and 20S proteasome activity (PI) was described using the simulated C_{plasma}:

Table 1 Patient characteristics

Age categories, years	1 to < 6	6 to < 12	12 to < 18	All patients
Total no. of patients	6	10	12	28
No. of PK samples	68	113	142	323
PK samples/patient (mean ± SD)	11.3 ± 3.77	11.3 ± 3.16	11.8 ± 2.17	11.7 ± 2.72
No. of PD samples	82	132	142	356
PD samples/patient (mean ± SD)	13.7 ± 4.27	13.2 ± 3.29	14.2 ± 2.66	13.7 ± 3.21
Age, years[a] (mean ± SD)	1.89 ± 0.93	8.59 ± 1.54	15.1 ± 1.58	9.94 ± 5.37
Height, m (mean ± SD)	82.3 ± 7.63	128.6 ± 8.15	155.0 ± 10.8	130 ± 29.4
Weight, kg (mean ± SD)	10.1 ± 1.88	27.7 ± 5.46	52.2 ± 9.83	34.4 ± 18.4
Body surface area, m^2 (mean ± SD)	0.47 ± 0.05	0.99 ± 0.12	1.49 ± 0.16	1.09 ± 0.42
Sex [*n* (%)]				
Male	4 (66.7)	8 (80.0)	4 (33.3)	16 (57.1)
Female	2 (33.3)	2 (20.0)	8 (66.7)	12 (42.9)

PK pharmacokinetic, *PD* pharmacodynamic, *SD* standard deviation

[a]Age at baseline

Table 2 Parameter estimates of bortezomib in the final pharmacokinetic model

	Units	Estimate	95% CI[a]	Shrinkage (%)
Population parameter				
Clearance (CL)[b]	L/h	6.32	3.76–9.83	–
Central volume of distribution (V_c)[b]	L	68.8	44.7–104	–
Intercompartment clearance (Q)[b]	L/h	34.5	21.8–53.0	–
Peripheral volume of distribution (V_p)[b]	L	622	388–1102	–
Equilibrium dissociation constant (K_D)	ng/mL	60.6	33.4–113	–
B_{max}	ng/mL	60.4	34.4–105	–
Between-subject variability				
B_{max}	CV%	51.8	39.2–70.7	3
Residual unexplained variability				
Proportional residual error	CV%	68.1	63.1–74.1	4

CI confidence interval, *CV%* percentage coefficient of variation, B_{max} maximal binding capacity

[a]95% CI values were obtained from sampling importance resampling

[b]Typical parameters provided for the median weight (i.e. 32 kg)

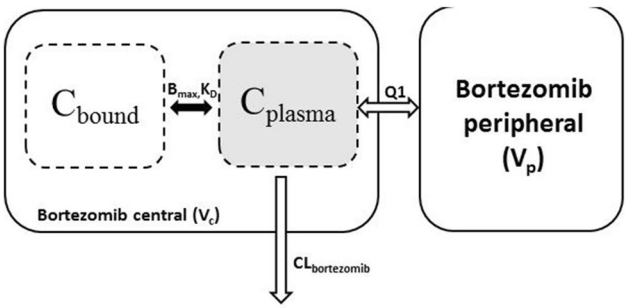

Fig. 1 Schematic representation of the semi-physiological PK model for bortezomib. Instantaneous equilibriums are depicted by the solid arrows, and open arrows represent the kinetic processes. Bortezomib concentrations are measured in the plasma compartment. *PK* pharmacokinetic

$$\mathrm{PI} = \mathrm{PI}_0 \times \left(1 - \left(\frac{E_{\max} \times C_{\mathrm{plasma}}^{\mathrm{Hill}}}{\mathrm{EC}_{50}^{\mathrm{Hill}} + C_{\mathrm{plasma}}^{\mathrm{Hill}}}\right)\right), \quad (7)$$

where PI_0 is the 20S proteasome activity at baseline, $E_{\max}$ and EC_{50} are the maximal decreases in 20S proteasome activity and bortezomib C_{plasma} at which the effect is half maximal, respectively, and Hill is the shape parameter.

Linear and $E_{\max}$ models were also investigated. Introduction of the Hill parameter resulted in a significantly improved fit and was thus retained in the final model. Exploration of an effect compartment model resulted in a large effect compartment rate estimate and no further improvement in model fit, which confirmed the adequateness of the direct effect model.

Table 3 Parameter estimates of 20S proteasome activity in the final pharmacodynamic model

	Units	Estimate	95% CI[a]	Shrinkage (%)
Population parameter				
20S proteasome activity at baseline (E_{base})	pmol AMC/s/mg protein	0.104	0.087–0.124	–
Maximal inhibitory effect (E_{max})	pmol AMC/s/mg protein	0.696	0.664–0.728	–
Sensitivity (EC_{50})	ng/mL	2.03	1.75–2.33	–
Shape parameter (Hill)	–	1.96	1.56–2.47	–
Between-subject variability				
20S proteasome activity at baseline (E_{base})	CV%	40.7	32.3–49.3	12
Residual unexplained variability				
Proportional residual error	CV%	20.7	19.2–22.6	4

CI confidence interval, *CV%* percentage coefficient of variation, *AMC* 7-amino-4-methycoumarin

[a]95% CI values were obtained from SIR

Univariate inclusion of covariates on the structural parameters did not improve the model fit. The final parameter estimates are summarized in Table 3. The maximal decrease in 20S proteasome activity was 0.696 pmol AMC/s/mg protein (95% CI 0.664–0.728), and 20S proteasome activity at baseline was 0.104 pmol AMC/s/mg protein (95% CI 0.087–0.124), with 40.7% (95% CI 32.3–49.3%) BSV.

3.4 Model Evaluation

The GOF plots and pcVPC showed that the final models adequately described the PK and variability of the observed bortezomib plasma concentrations for each treatment week (Figs. 2, 3). This indicates that the incorporation of saturable binding of bortezomib in the central compartment adequately explained the nonlinearity in the observed PK profiles. A trend towards higher conditional weighted residual (CWRES) values for higher concentrations was observed. Nevertheless, the 95% CIs that were obtained by SIR were reasonably narrow, except for K_D and B_{max}, which can be explained by the fact that detailed information on target binding was not available.

The pcVPC of the PD model (Fig. 3) showed an overprediction of the 20S proteasome activity at 8 h postdose. In addition, the CWRES versus time plot showed a slight trend towards negative CWRES values after the third administration. Nevertheless, the GOF plots (Fig. 2) and pcVPC showed an adequate description of the 20S proteasome activity measured immediately after dose administration until 8 h postdose, by the final PD model.

4 Discussion

The complex PK of bortezomib were adequately described using a two-compartment model with linear elimination. Incorporation of nonlinear binding in the central compartment significantly improved the model fit and explained the higher plasma concentrations in the second week of treatment. The distribution in whole blood was previously investigated in MM patients [23]. The bortezomib concentration in whole blood was found to be approximately threefold higher than that in plasma. In addition, whole blood concentrations increased during treatment, suggesting a limited

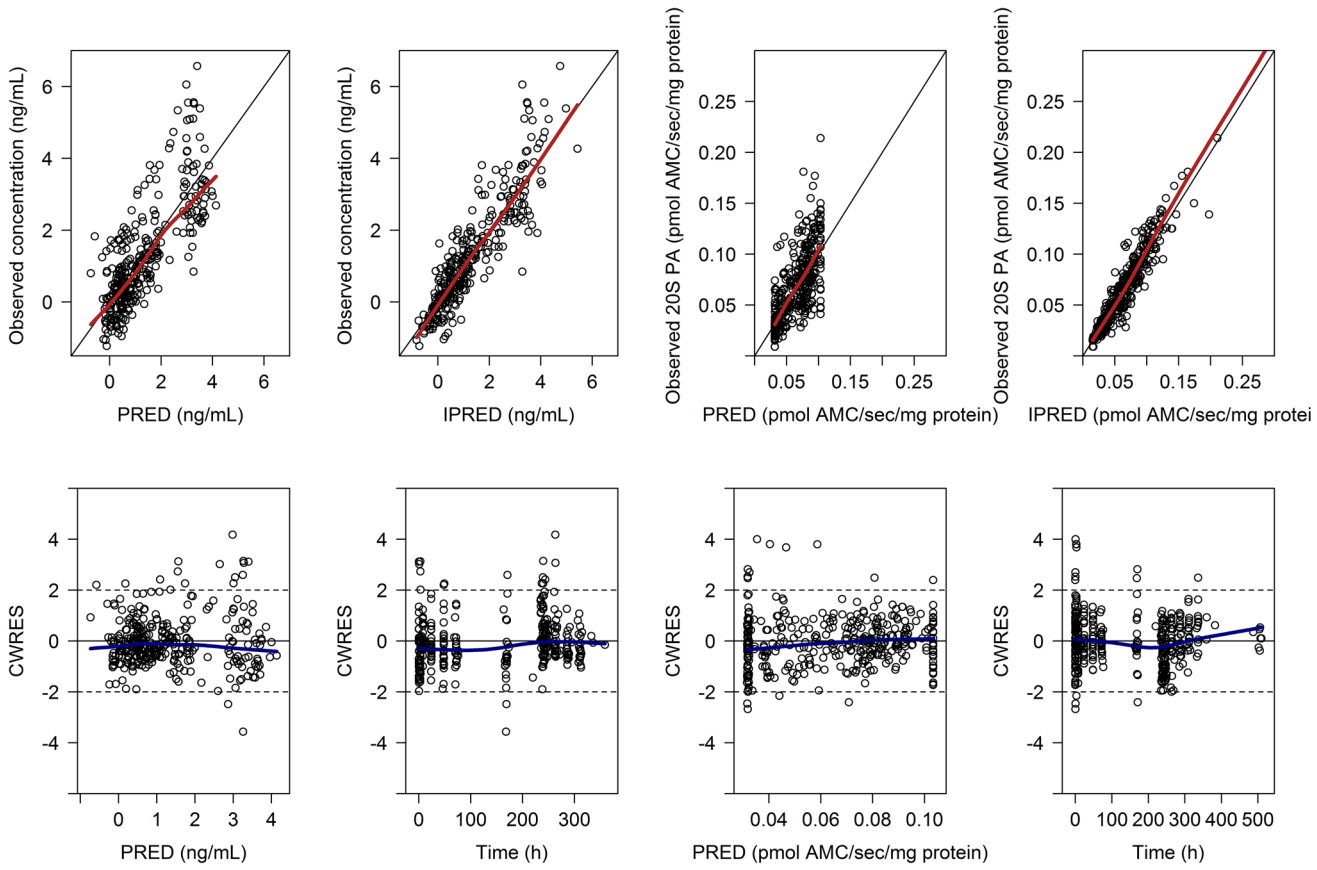

Fig. 2 Goodness-of-fit plots of the final PK and PD models. Model-predicted log-transformed bortezomib concentrations (ng/mL) and 20S PA, including individual (IPRED) and population predictions (PRED) vs. observed values and CWRES vs. time after the first dose and PRED. *PK* pharmacokinetic, *PD* pharmacodynamic, *PA* proteasome activity, *CWRES* conditional weighted residuals

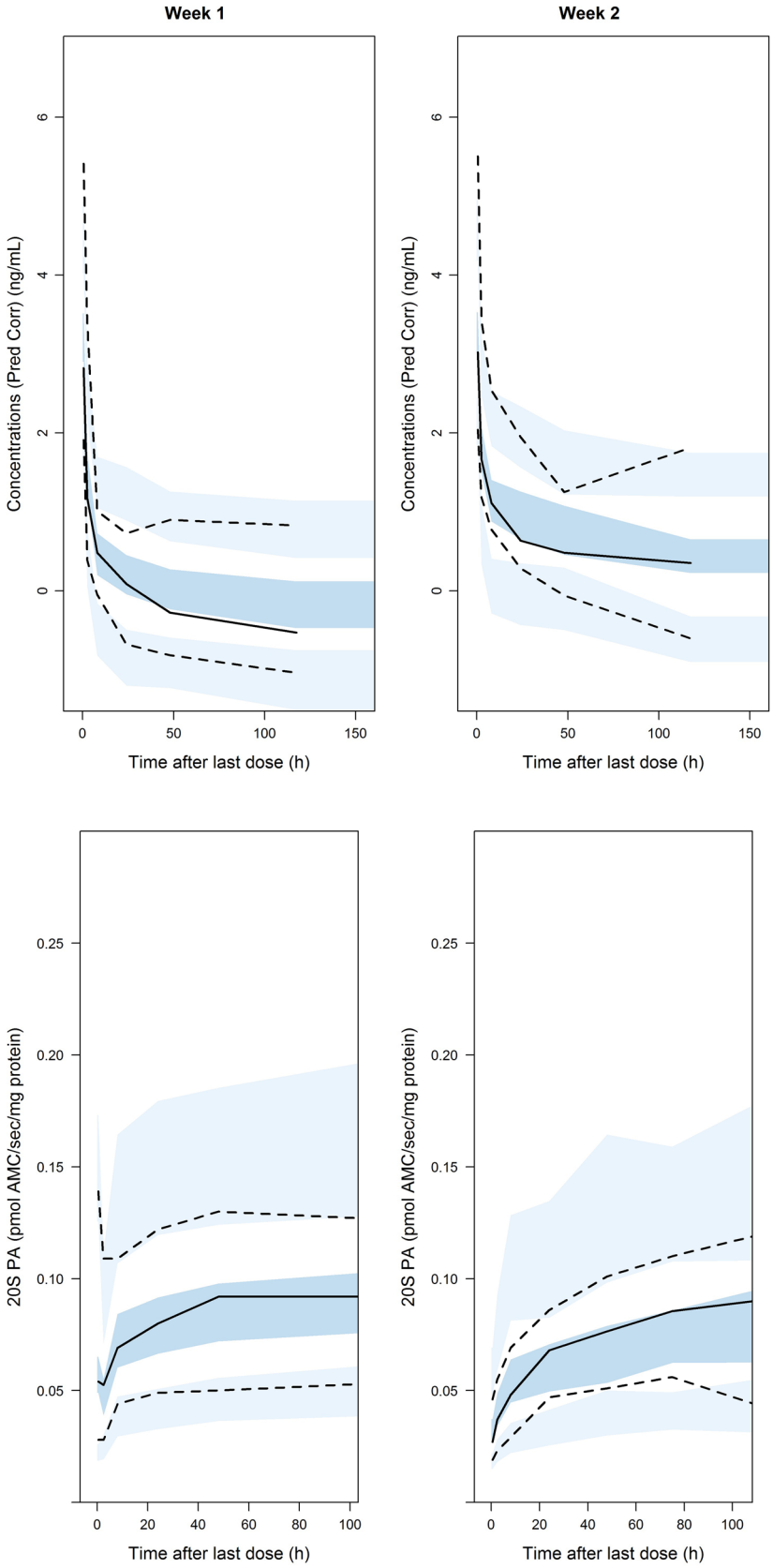

Fig. 3 Prediction-corrected visual predictive check of the final PK (upper panels) and PD (lower panels) model stratified by treatment week. Solid lines and darker blue areas represent the median observed values and simulated 80% CIs, and dashed lines and light blue areas represent the 10% and 90% percentiles of the observed values and 80% CIs of the simulated percentiles ($n = 1000$). *PK* pharmacokinetic, *PD* pharmacodynamic, *CIs* confidence intervals

accumulation of bortezomib in red blood cells. Furthermore, Zhang and Mager developed a physiologically based PK model incorporating saturable target binding to capture the nonlinear bortezomib tissue distribution in mice. Bortezomib showed reversible high affinity for binding to the proteasome. As a result of high abundance of the proteasome in erythrocytes, and slow dissociation kinetics, bortezomib is expected to rapidly bind but slowly dissociate from proteasome in erythrocytes, and thus accumulate in red blood cells [12]. Notwithstanding, it could be hypothesized that bortezomib may bind to other proteins present in human plasma. Our semi-physiological model is the first description of the nonlinearity in bortezomib PK in both children and adults. Although the current data were obtained from a trial in children, our modeling approach could be used for other drugs that are used in the treatment of both adult and pediatric patients that show distribution to erythrocytes.

In the final PK model, large residual unexplained variability was observed. This may be due to inconsistencies in sample collection and registration of dosing and sampling records. Given the fast decline in concentrations within the first hour after administration, small deviations between the actual and registered administration and sampling times may easily lead to high residual variability. Nevertheless, the registered administration times were used in the analysis. Additionally, we were unable to include BSV or covariate effects on structural parameters other than BSV on B_{max}, and body weight on all volumes of distribution and clearance parameters. Despite this limitation, the diagnostic plots and pcVPC show that the observed concentrations are well captured by the model.

The 20S proteasome activity versus time profile following bortezomib administration was well-described by an inhibitory sigmoidal E_{max} model, indicating that 20S proteasome activity in peripheral whole blood samples is directly related to bortezomib C_{plasma}. Large variability in baseline 20S proteasome activity was observed, which is demonstrated by the 40.6% BSV on baseline effect in our model. The covariates that were available were unable to explain this variability.

The overprediction of the 20S proteasome activity at 8 h postdose can be explained by the use of the direct effect model with simulated C_{plasma} as input. Some patients did not recover to baseline before the next dose was administered. At this time, the concentrations in plasma are low, while there is still drug bound to the proteasome. Direct effect models using estimated C_{bound} were explored but could not be estimated with adequate precision.

Our results are in line with the structural results from the previously published pediatric population PK analysis of bortezomib [10]. A population clearance of 9.59 L/h, and large volumes of distribution of 10.0, 32.5, and 975 L for V1, V2, and V3, respectively, were reported. We were not able to identify BSV on parameters other than B_{max}, as has been done by Hanley et al. [10]. This is most likely a result of the limited data that were available for our analysis and the complexity of our structural model. Despite our relatively small sample size, our model is superior to this previously published model in incorporating data from both treatment weeks into a semi-physiological approach, thereby explaining the observed nonlinearity in PK. In the previously published empirical model, only data from the first week of treatment were included. Hanley et al. identified a covariate effect of BSA on CL and the intercompartmental clearance between the first and third compartment. We used total body weight for allometric scaling of all volumes of distribution and clearance parameters to account for changes in body size. Given the limited number of subjects, and consequently the limited weight range in our cohort, fixed allometric exponents were used [14]. An additional maturation effect using PMA could not be identified when weight was accounted for, which is most likely due to the lack of patients younger than 2 years of age in our cohort. Nevertheless, to our knowledge, this is the first model for bortezomib combining PK and PD.

A comparison of the results from our PD model with previous reports cannot be made as these analyses used relative 20S proteasome inhibition to describe the PD effect [6, 24]. Our data showed that baseline 20S proteasome activity varied widely between patients, and hence it was not rational to use relative 20S proteasome inhibition instead of 20 proteasome activity.

5 Conclusion

We successfully developed a model that describes the population PK/PD of bortezomib in pediatric patients with rALL. The observed nonlinearity could be explained by saturable distribution of bortezomib within the central compartment, which is presumably caused by saturable binding to erythrocytes.

Acknowledgements The authors thank the investigators, research staff, and patients for their participation in this study.

Compliance with Ethical Standards

Funding This clinical study was supported by the Dutch Foundation Children Cancer-Free (clinical research support) and by Janssen Pharmaceuticals (clinical research support and free drug).

Conflict of interest A. Baruchel has declared links of interest with Amgen, Celgene, Jazz, Novartis, Servier, and Shire. J. M. Janssen, T. P. C. Dorlo, D. Niewerth, A. J. Wilhelm, C. M. Zwaan, J. H. Beijnen, A. Attarbaschi, F. Fagioli, T. Klingebiel, B. De Moerloose, G. Palumbo, A. von Stackelberg, G. J. L. Kaspers, and A. D. R. Huitema have no conflicts of interest to declare, other than the funding mentioned previously.

References

1. Pui C-H, Yang JJ, Hunger SP, Pieters R, Schrappe M, Biondi A, et al. Childhood acute lymphoblastic leukemia: progress through collaboration. J Clin Oncol. 2015;33:2938–48.
2. Moreno L, Pearson ADJ, Paoletti X, Jimenez I, Geoerger B, Kearns PR, et al. Early phase clinical trials of anticancer agents in children and adolescents—an ITCC perspective. Nat Rev Clin Oncol. 2017;14:497–507.
3. Bross PF, Kane R, Farrell AT, Abraham S, Benson K, Brower ME, et al. Approval summary for bortezomib for injection in the treatment of multiple myeloma. Clin Cancer Res. 2004;10(2 Pt 1):3954–64.
4. Tan CRC, Abdul-Majeed S, Cael B, Barta SK. Clinical pharmacokinetics and pharmacodynamics of bortezomib. Clin Pharmacokinet. 2019;58(2):157–68.
5. Houghton PJ, Morton CL, Kolb EA, Lock R, Carol H, Reynolds CP, et al. Initial testing (stage 1) of the proteasome inhibitor bortezomib by the pediatric preclinical testing program. Pediatr Blood Cancer. 2008;50:37–45.
6. Reece DE, Sullivan D, Lonial S, Mohrbacher AF, Chatta G, Shustik C, et al. Pharmacokinetic and pharmacodynamic study of two doses of bortezomib in patients with relapsed multiple myeloma. Cancer Chemother Pharmacol. 2011;67:57–67.
7. Horton TM, Pati D, Plon SE, Thompson PA, Bomgaars LR, Adamson PC, et al. A phase 1 study of the proteasome inhibitor bortezomib in pediatric patients with refractory leukemia: a Children's Oncology Group study. Clin Cancer Res. 2007;13:1516–22.
8. Muscal JA, Thompson PA, Horton TM, Ingle AM, Ahern CH, McGovern RM, et al. A Phase I trial of vorinostat and bortezomib in children with refractory or recurrent solid tumors: a Children's Oncology Group Phase I Consortium Study (ADVL0916). Pediatr Blood Cancer. 2013;60:390–5.
9. Blaney SM, Bernstein M, Neville K, Ginsberg J, Kitchen B, Horton T, et al. Phase I study of the proteasome inhibitor bortezomib in pediatric patients with refractory solid tumors: a Children's Oncology Group Study (ADVL0015). J Clin Oncol. 2004;22:4804–6.
10. Hanley MJ, Mould DR, Taylor TJ, Gupta N, Suryanarayan K, Neuwirth R, et al. Population pharmacokinetic analysis of bortezomib in pediatric leukemia patients: model-based support for body surface area-based dosing over the 2- to 16-year age range. J Clin Pharmacol. 2017;57(9):1183–93.
11. Kaspers GJL, Niewerth D, Wilhelm BAJ, Scholte-van Houtem P, Lopez-Yurda M, Berkhof J, et al. An effective modestly intensive re-induction regimen with bortezomib in relapsed or refractory paediatric acute lymphoblastic leukaemia. Br J Haematol. 2018;181(4):523–7.
12. Zhang L, Mager DE. Physiologically-based pharmacokinetic modeling of target-mediated drug disposition of bortezomib in mice. J Pharmacokinet Pharmacodyn. 2015;42:541–52.
13. West GB, Brown JH, Enquist BJ. A general model for the origin of allometric scaling laws in biology. Science. 1997;276(5309):122–6.
14. Anderson BJ, Holford NHG. Mechanism-based concepts of size and maturity in pharmacokinetics. Annu Rev Pharmacol Toxicol. 2008;48:303–32.
15. Germovsek E, Barker C, Sharland M, Standing JF. Scaling clearance in paediatric pharmacokinetics: all models are wrong, which are useful? Br J Clin Pharmacol. 2016;83:777–90.
16. Upton RN, Mould DR. Basic concepts in population modeling, simulation, and model-based drug development: part 3-introduction to pharmacodynamic modeling methods. CPT Pharmacomet Syst Pharmacol. 2014;3:e88.
17. Nguyen T, Mouksassi M-S, Holford N, Al-Huniti N, Freedman I, Hooker A, et al. Model evaluation of continuous data pharmacometric models: metrics and graphics. CPT Pharmacomet Syst Pharmacol. 2017;6:87–109.
18. Dosne A-G, Bergstrand M, Karlsson MO. An automated sampling importance resampling procedure for estimating parameter uncertainty. J Pharmacokinet Pharmacodyn. 2017;44:509–20.
19. Lindbom L, Ribbing J, Jonsson EN. Perl-speaks-NONMEM (PsN)—a Perl module for NONMEM related programming. Comput Methods Programs Biomed. 2004;75:85–94.
20. Keizer RJ, van Benten M, Beijnen JH, Schellens JHM, Huitema ADR. Pirana and PCluster: a modeling environment and cluster infrastructure for NONMEM. Comput Methods Programs Biomed. 2011;101:72–9.
21. Beal S, Boeckmann A, Sheiner L. NONMEM user guides. San Francisco: University of California, San Francisco; 1988.
22. Team RC. R: a language and environment for statistical computing. Vienna: R Foundation for Statistical Computing; 2009.
23. Osawa T, Naito T, Kaneko T, Mino Y, Ohnishi K, Yamada H, et al. Blood distribution of bortezomib and its kinetics in multiple myeloma patients. Clin Biochem. 2014;47:54–9.
24. Moreau P, Karamanesht II, Domnikova N, Kyselyova MY, Vilchevska KV, Doronin VA, et al. Pharmacokinetic, pharmacodynamic and covariate analysis of subcutaneous versus intravenous administration of bortezomib in patients with relapsed multiple myeloma. Clin Pharmacokinet. 2012;51:823–9.

Affiliations

Julie M. Janssen[1] · T. P. C. Dorlo[1] · D. Niewerth[2] · A. J. Wilhelm[3] · C. M. Zwaan[4,5,16] · J. H. Beijnen[1,6] · A. Attarbaschi[7,8] · A. Baruchel[9,16] · F. Fagioli[10] · T. Klingebiel[11] · B. De Moerloose[12] · G. Palumbo[13] · A. von Stackelberg[14] · G. J. L. Kaspers[2,4] · A. D. R. Huitema[1,15]

1 Department of Pharmacy and Pharmacology, Netherlands Cancer Institute-Antoni van Leeuwenhoek, Plesmanlaan 121, 1066 CX Amsterdam, The Netherlands

2 Department of Pediatric Oncology/Hematology, VU University Medical Center, Amsterdam, The Netherlands

3 Department of Clinical Pharmacology and Pharmacy, VU University Medical Center, Amsterdam, The Netherlands

4 Princess Maxima Center for Pediatric Oncology, Utrecht, The Netherlands

5 Department of Pediatric Oncology/Hematology, Erasmus-MC Sophia Children's Hospital, Rotterdam, The Netherlands

6 Utrecht Institute for Pharmaceutical Sciences (UIPS), Utrecht University, Utrecht, The Netherlands

7 Department of Pediatric Hematology and Oncology, St. Anna Children's Hospital, Vienna, Austria

8 Department of Pediatrics and Adolescent Medicine, Medical University Vienna, Vienna, Austria

[9] Department of Pediatric Hematology, Hopital Saint Louis, Paris, France

[10] Università degli Studi di Torino, Turin, Italy

[11] Department of Pediatrics, University Hospital Frankfurt, Frankfurt am Main, Germany

[12] Department of Pediatrics, Ghent University Hospital, Ghent, Belgium

[13] Ospedale Pediatrico Bambino Gesù, Rome, Italy

[14] Department of Pediatric Oncology/Hematology, Charité Universitätsmedizin, Berlin, Germany

[15] Department of Clinical Pharmacy, University Medical Center Utrecht, Utrecht University, Utrecht, The Netherlands

[16] ITCC Consortium, Paris, France